This information is current as of December 10, 2013.

Cognate Peptide–MHC Complexes Are Expressed as Tightly Apposed Nanoclusters in Virus-Infected Cells To Allow TCR Crosslinking

María Ferez, Mario Castro, Balbino Alarcon and Hisse M. van Santen

J Immunol published online 4 December 2013
http://www.jimmunol.org/content/early/2013/12/04/jimmunol.1301224

The Journal of Immunology is published twice each month by The American Association of Immunologists, Inc., 9650 Rockville Pike, Bethesda, MD 20814-3994.

Print ISSN: 0022-1767 Online ISSN: 1550-6606.

Published December 4, 2013, doi:10.4049/jimmunol.1301224

Cognate Peptide–MHC Complexes Are Expressed as Tightly Apposed Nanoclusters in Virus-Infected Cells To Allow TCR Crosslinking

María Ferez,* Mario Castro,† Balbino Alarcon,* and Hisse M. van Santen*

Antigenic T cell stimulation requires interaction between the TCR of the T cell and cognate peptide–MHC molecules presented by the APC. Although studies with TCR-specific Abs and soluble peptide–MHC ligands have shown that the TCR needs to be crosslinked by two or more ligands to induce T cell stimulation, it is not understood how several MHC molecules loaded with the cognate antigenic peptide can produce crosslinking under physiological conditions. We show at the molecular level that large clusters of cognate peptide–MHC are formed at the surface of murine professional and nonprofessional APCs upon virus infection and that these clusters impinge on the stimulatory capacity of the APC. These clusters are formed by tight apposition of cognate peptide–MHC complexes in a configuration that is compatible with simultaneous engagement of two or more TCRs. This suggests that physiological expression of Ag allows formation of multivalent ligands for the TCR that permit TCR crosslinking and T cell activation. ***The Journal of Immunology*****, 2014, 192: 000–000.**

The interaction between cognate peptide–MHC (pMHC) complexes and the TCR is a key event in activating the adaptive immune response. T cells have very high sensitivity for Ag, needing only few cognate pMHC complexes presented by APCs to become activated (1–3). However, the pMHC–TCR interaction is of low affinity (4–6), making it difficult to explain how T cells achieve high sensitivity. We previously showed that the TCR was organized in nanoclusters prior to Ag engagement and that this clustering endowed T cells with higher sensitivity (7, 8). Furthermore, it has long been recognized that experimental TCR ligands, such as TCR-specific Abs and soluble pMHC complexes, need to be at least bivalent to be capable of stimulating T cells (9, 10). Taken together, these observations suggest that T cell stimulation is guided by multivalent interactions. It is therefore relevant to determine whether multivalent TCR ligands exist under physiological conditions, that is, multivalent cognate pMHC complexes at the plasma membrane of APCs.

MHC class II molecules have been detected by means of confocal microscopy in discrete plasma membrane domains in a variety of cell lines (11–13). Where tested, these domains have been shown to depend on cholesterol for their integrity, suggesting that they are formed by lipid rafts. Other authors have described that MHC class II molecules can form alternative domains with tetraspanins in both cell lines and primary dendritic cells and that these domains are enriched for particular peptides (14). Disruption of MHC class II domains with cholesterol-sequestering agents or saponin leads to reduced stimulatory capacity of the treated APCs (11). This suggests that these MHC-enriched regions are important for providing sensitivity to the T cells, although such experiments cannot exclude that additional alterations caused by the drug treatment are involved in reducing the stimulatory capacity. Similarly, clusters of MHC class I molecules have been detected at the plasma membrane of cell lines by means of confocal microscopy and fluorescence resonance energy transfer analysis (13, 15). Bigger MHC class I clusters seem to enhance stimulatory potential because increase of their size by pharmacological means and MHC class I crosslinking correlates with enhanced T cell recognition (16).

The experiments described above show that clusters of MHC molecules do exist and may modulate T cell activation and responsiveness, but they have not provided direct evidence whether MHC molecules presenting identical peptides can be found within such clusters. In this study, we have used a technique that permits molecular resolution of the distribution of cell surface molecules to study the distribution of a defined pMHC complex at the cell surface of virus-infected cells and to compare it with the cluster distribution of MHC class I molecules loaded with the corresponding exogenously provided soluble antigenic peptide.

Materials and Methods

Cells and virus

The murine lymphoma EL4 (17) was grown in RPMI 1640 supplemented with 5% FCS, 2 mM L-glutamine, and 100 U/ml streptomycin/penicillin (RPMI-5). The acute T cell leukemia Jurkat (18) was grown in RPMI-5. EL4-derived E.G7-OVA cells (19) were grown in RPMI-5 supplemented with 10 μM 2-ME and 0.1 mg/ml G418. Bone marrow–derived dendritic cells were obtained by culturing bone marrow cells for 1 wk in RPMI-10 supplemented with 10 mM sodium pyruvate, 50 μM 2-ME, and 20 ng/ml GM-CSF according to established protocols (20). The full-length OVA encoding modified vaccinia virus Ankara ([MVA-OVA]; a gift of

*Departamento de Biología Celular e Inmunología, Centro Biología Molecular Severo Ochoa, Consejo Superior de Investigaciones Científicas/Universidad Autónoma de Madrid, 28049 Cantoblanco, Spain; and †Grupo Interdisciplinar de Sistemas Complejos, Escuela Técnica Superior de Ingeniería, Universidad Pontificia Comillas de Madrid, 28015 Madrid, Spain

Received for publication May 20, 2013. Accepted for publication November 1, 2013.

This work was supported by Ministerio de Economia y Competitividad Grants BFU2009-08009 (to H.M.v.S.), SAF2010-14912 (to B.A.), and FIS2009-12964-C05-03 (to M.C.). M.F. was a recipient of a Formación de Personal Investigador predoctoral fellowship (Grant BES-2007-15570) from the Ministerio de Ciencia e Innovación.

Address correspondence and reprint requests to Dr. Balbino Alarcon and Dr. Hisse M. van Santen, Centro Biología Molecular Severo Ochoa, Calle Nicolás Cabrera 1, 28049 Cantoblanco, Spain. E-mail addresses: balarcon@cbm.uam.es (B.A.) and hvansanten@cbm.csic.es (H.M.v.S.)

The online version of this article contains supplemental material.

Abbreviations used in this article: IPR, inverse participation ratio; K^bOVAp, MHC class I H-$2K^b$ molecule loaded with the OVA-derived SIINFEKL ($OVA_{257–264}$) peptide; MVA, modified vaccinia virus Ankara; MVA-OVA, OVA encoding MVA; NIPR, normalized inverse participation ratio; OVAp, synthetic OVA peptide SIINFEKL; pMHC, peptide–MHC; TfR, transferring receptor; WT, wild-type.

Drs. E. Schwantes and G. Sutter, Paul Ehrlich Institute, Langen, Germany) (21) and the parental strain MVA; obtained via Dr. M. Esteban, Centro Nacional de Biotecnología, Madrid, Spain) were propagated and titrated in BHK-21 cells according to published methods (22).

Mice

OT-1 mice, expressing a transgenic TCR specific for the OVA-derived peptide SIINFEKL ($OVA_{257–264}$) bound to H-2K^b molecules (23), were maintained in the animal facility of the Centro de Biología Molecular Severo Ochoa in accordance with guidelines of the current legislation.

Abs and reagents

Purified human MHC class I–specific mAb W6/32 (24) and ascites of human transferrin receptor–specific mAb FG1/5 (25) were used at previously determined saturating conditions for staining. The mAb 25D1.16 (26) was obtained in biotinylated or purified form from eBioscience. The vaccinia-specific rabbit serum was a gift of Dr. A. Alcami (Centro Biología Molecular Severo Ochoa, Madrid, Spain). Fluorophore-conjugated and biotinylated mAbs specific for murine TCR Vα2, CD8, H-2K^b (clone AF6-88.5), and H-2D^b (clone B22.249) were from BD Pharmingen. Fluorophore-conjugated anti-murine IFN-γ was obtained from Miltenyi Biotec. Alexa Fluor 555–coupled donkey anti-mouse IgG and Alexa Fluor 488–coupled donkey anti-rabbit IgG secondary Abs and TO-PRO-3 nuclear dye were from Invitrogen. Methyl-β-cyclodextrin was purchased from Sigma-Aldrich. Synthetic OVA peptide SIINFEKL (OVAp) was generated by the proteomics facility of the Centro Biología Molecular Severo Ochoa by Fmoc chemistry.

Immunofluorescent staining

Bone marrow dendritic cells, directly grown on glass coverslips, and EL4 and E.G7-OVA cells, adhered to coverslips pretreated with 50 μg/ml poly-L-lysine, were fixed with 2% paraformaldehyde before staining with the indicated primary Abs and appropriate secondary reagents. After embedding in Mowiol, cells were imaged with LSM 510 Meta and LSM 710 confocal microscopes (Carl Zeiss Jena) with ×63/1.4 Plan Apo oil immersion objective lens, and acquired images were analyzed by an LSM image browser (Carl Zeiss Jena) and Fiji (27) software.

Normalized inverse participation ratio

To quantify the degree of homogeneity of the distribution of the K^{b}OVAp complexes at the cell surface of virus-infected and peptide-incubated EL4 cells, we make use of the concept of the inverse participation ratio (IPR) (28), commonly used in quantum material science to ascertain the degree to which a material behaves as a metal or an insulator. This ratio considers a certain continuum or discrete distribution of probability p_i defined as the probability at spatial position i (or in the continuum limit, x).

The IPR is defined as

$$IPR = \left(\sum_i^N p_i^2\right)^{-1} \quad (1)$$

where N is the number of points where the distribution has been measured. The rationale under Eq. 1 is the following: for a homogeneous distribution, $p_i = 1/N$ (namely, the distribution is flat; in that case, $IPR = N$). On the contrary, when the distribution is 0 except in position k, then $p_{i\neq k} = 0$ and $p_k = 1$. In this case, $IPR = 1$.

For a large number of points, and for the sake of comparing different data sets (with, also, a different number of points N where the distribution has been measured), it is more convenient to define a normalized version of Eq. 1, namely

$$NIPR = \frac{1}{N}\left(\sum_i^N p_i^2\right)^{-1} \quad (2)$$

Now the range would be between $1/N \approx 0$ (highly peaked distribution) and 1 (flat or homogeneous distribution).

Using the segmented line tool of the Fiji platform (27), a 5-pixel-wide line (pixel size, 0.14 μm) was drawn around the plasma membrane of midplane optical sections of MVA-OVA–infected or OVAp-incubated EL4 cells, E.G7-OVA cells, or primary dendritic cells stained with K^{b}OVAp- or K^b-specific Abs. After straightening this line, a plot profile was obtained, giving the averaged intensity values of staining in each point of the circumference. Averaged intensity values (p_i) and the number of measuring points on the circumference (N) were used to calculate the NIPR according to Eq. 2.

Replica preparation and transmission electron microscopy

Cells fixed with 2% paraformaldehyde were labeled with primary Abs and 10-nm colloidal gold–conjugated protein A (Cell Microscopy Center, University of Utrecht, Utrecht, The Netherlands). In the case of labeling with the 25D1.16 mAb (mouse IgG1), a bridging hamster anti-mouse IgG was used to overcome the low affinity of protein A for murine IgG1 Abs. Replica generation was done as previously described (7, 8). Replicas were analyzed on a JEOL 1010 transmission electron microscope operating at 80 kV, and images were acquired with a TemCAM F416 camera operated by EM-MENU software (Tietz Video and Image Processing Systems).

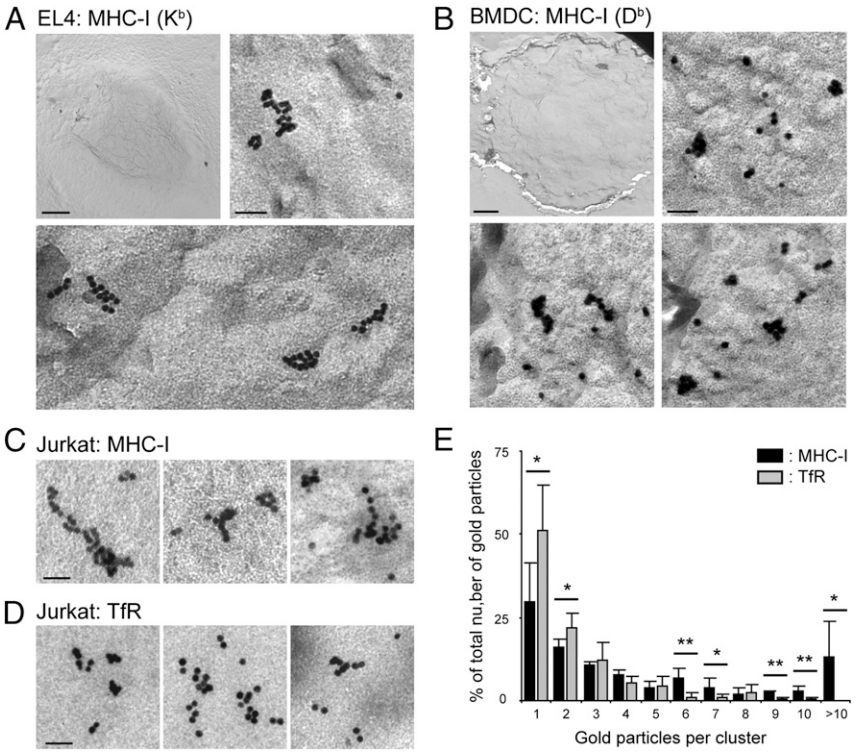

FIGURE 1. Detection of clusters of tightly packed MHC class I molecules at the cell surface membrane. (**A**) Transmission electron microscopy images of cell surface replicas of EL4 cells labeled with the K^b-specific mAb AF6-88.5 and protein A conjugated to 10-nm colloidal gold (PAG10). An image corresponding to the whole cell was obtained by automated tiling of images taken at 10,000 magnification of adjacent areas of the replica. Scale bars: whole cell image, 2 μm; details, 50 nm. (**B**) Cell surface replicas of bone marrow–derived dendritic cells labeled with the D^b-specific Ab B22.249 and PAG10. Image corresponding to whole cell taken at 5,000 magnification, details at 100,000. Scale bars: whole cell image, 2 μm; details, 50 nm. (**C** and **D**) Details of cell surface replicas of Jurkat cells labeled with the MHC class I–specific mAb W6/32 and PAG10 (C) or the transferring receptor–specific mAb FG1/5 and PAG10 (D). Images were taken at 100,000 magnification. Scale bars: 50 nm. (**E**) Comparison of the size of gold clusters on replicas of Jurkat cells labeled with anti-MHC class I and anti-TfR Abs. Quantification of six anti–MHC class I–labeled cells (4518 particles) and four anti-TfR–labeled cells (2303 particles) is shown. Statistical significance of differences observed for each cluster size was calculated with a two-tailed, unpaired t test. $^*p < 0.05$, $^{**}p < 0.01$.

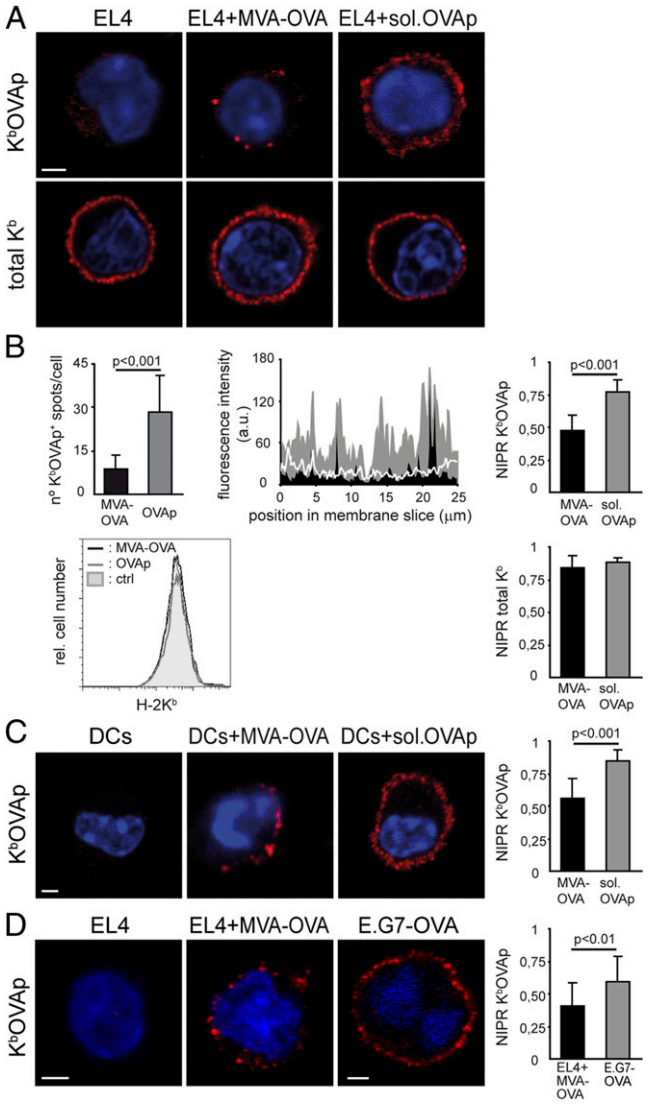

FIGURE 2. MHC class I molecules presenting a peptide generated upon viral infection are concentrated in clusters. (**A**) Confocal images of EL4 cells that had either been infected with the MVA-OVA virus at 10 PFU/cell or had been incubated with 1 μM soluble OVAp and untreated EL4 cells followed by labeling with the K^bOVAp-specific mAb 25D1.16 or the total K^b-specific mAb AF6-88.5 and an anti-mouse Alexa Fluor 555–conjugated Ab and stained with TO-PRO to detect nuclei. Representative midplane optical sections from one of three experiments are shown. (**B**) Quantification of label distribution. The *upper left panel* shows the number of K^bOVAp spots (mean ± SD) in membrane of midplane sections of 30 MVA-OVA–infected and 41 OVAp-incubated EL4 cells as determined with the "Analyze Particles" plugin of Fiji. The *upper middle panel* shows an overlay of intensity profiles of membrane labeling of representative MVA-OVA–infected (black), OVAp-incubated (gray), and control (white line) EL4 cells. The *upper right panel* shows quantification of label distribution of 16 MVA-OVA–infected and 12 OVAp-treated EL4 cells using the NIPR. The *lower left panel* shows intensity of total K^b labeling of the indicated cells (gated for live cells) as determined by flow cytometry. The *lower right panel* represents the NIPR (mean ± SD) of total K^b labeling of 12 MVA-OVA–infected and 12 OVAp-incubated EL4 cells. (**C**) Confocal images of bone marrow–derived dendritic cells that had either been infected 6 h before with the MVA-OVA virus at 5 PFU/cell, had been incubated with 1 μM soluble OVAp, or had been left untreated, followed by labeling with mAb 25D1.16 and TO-PRO. Representative midplane optical sections are shown. The graph on the right shows the NIPR (mean ± SD) of 25D1.16 labeling intensity for 7 MVA-OVA–infected and 13 OVAp-incubated dendritic cells. (**D**) Imaging and quantification of K^bOVAp distribution in MVA-OVA–infected EL4 cells and E.G7-OVA cells. Confocal images show representative midplane sections of 25D1.16-labeled cells. The graph shows the NIPR (mean ± SD) of 25D1.16-labeled MVA-OVA–infected EL4 (n = 18) and E.G7-OVA (n = 14) cells. Scale bars in (A), (C), and (D), 2 μm. Statistical significance of differences for all experiments was calculated with a two-tailed, unpaired Student t test. Staining pattern and NIPR calculations were confirmed in one independent experiment each for all experiments shown. See also Supplemental Figs. 1 and 2.

Flow cytometry

Cells were stained with the indicated directly conjugated and biotinylated primary Abs in PBS supplemented with 1% BSA and 0.02% sodium azide, and where applicable with the appropriate secondary reagents. For intracellular staining for IFN-γ, cells were fixed and permeabilized with a commercial kit according to the manufacturer's recommendations (Cytofix/Cytoperm; BD Pharmingen). Stained cells were acquired on a FACSCalibur flow cytometer (Becton Dickinson) and data were analyzed with FlowJo software (Tree Star).

In vitro T cell activation assays

EL4 cells (1×10^5) were seeded in 96-well round bottom plates in RPMI-10 supplemented with 10 mM sodium pyruvate and 10 μM 2-ME and infected with MVA-OVA at 10 PFU/cell, or infected with MVA-wild-type (WT) at the same ratio and incubated with graded amount of soluble OVAp. After 6 h cultures were washed and 2×10^5 OT-1 T cells, isolated from the superficial and mesenteric lymph nodes of OT-1 mice, were added. Cultures were grown for 2 d and during the last 4 h 3 μg/ml brefeldin A was added (eBioscience).

Results

Clustering of MHC class I molecules in primary cells and cell lines

We first analyzed clustering of the general population of MHC class I molecules at the cell surface of primary cells and cell lines. We used our previously established approach of cell surface replica generation of fixed cells labeled with primary Abs and colloidal gold–conjugated secondary reagents in combination with transmission electron microscopy (7, 8). This approach permits molecular resolution of the cell surface localization of endogenous proteins and, in contrast to most high-resolution light microscopy techniques, visualizes the cell surface membrane opposite to the one in contact with the experimental support. This avoids possible concerns about contact-induced clustering of cell surface molecules (29).

We prepared cell surface replicas of the murine thymoma EL4, murine bone marrow–derived dendritic cells, and the human T cell lymphoma Jurkat. All cells had been fixed with paraformaldehyde prior to labeling with Abs specific for MHC class I and 10 nm colloidal gold–conjugated protein A on ice. Analysis by electron microscopy revealed clusters of gold particles in replicas of all three cell types (Fig. 1A–C), indicating that clusters of MHC class I molecules were present on the surface of all cells tested. The distance between neighboring gold particles was smaller than the resolving power of the electron microscope under the conditions used (<1 nm). Taking into account the lateral dimensions of the peptide-binding α_1 and α_2 domain of the class I molecule (~4×5 nm^2) (30), the spacing of the gold particles indicated that the distance between adjacent MHC class I molecules within such clusters was equal to or less than the size of a single MHC class I molecule. The observed cluster size ranged mainly between 2 and 20 gold particles, but in few occasions larger clusters were detected. The relative inefficiency of detection of the replica technique (7) did not permit us to determine the absolute size of clusters, and these sizes therefore represented a minimum estimate.

Comparison of the distribution of MHC class I molecules and the transferrin receptor (TfR) on the cell surface of Jurkat T cells indicated that TfR clustered to a significantly lesser extent (Fig. 1C–E),

even without taking into account that TfR is a disulfide-linked homodimer and that two adjacent gold particles could therefore represent labeling of the same homodimer. This suggests that the degree of clustering of cell surface molecules varies for different cell surface receptors. Thus, MHC class I molecules seem to form larger pre-existing clusters, as observed for the TCR (31, 32), whereas TfR appears to form smaller clusters, similar to CD25 (32).

Knowing that the general population of MHC class I complexes formed clusters of tightly apposed molecules and given the requirement of multivalency for experimental TCR ligands, it was of interest to study the distribution of cognate pMHC complexes at the cell surface of APCs.

Detection of cognate pMHC clusters after viral infection

EL4 cells were infected with rMVA expressing full-length OVA (MVA-OVA) (21). Immunoblotting of cell lysates at different time points after infection showed that these cells were productively infected and that the OVA protein was expressed (Supplemental Fig. 1A). Six hours after the beginning of infection the cells were labeled with mAb 25D1.16 (26), specific for the OVA-derived peptide SIINFEKL ($OVA_{257–264}$) bound to the MHC class I molecule H-$2K^b$ (referred to as K^bOVAp), and analyzed by confocal microscopy. Double labeling with an antiserum specific for vaccinia virus and the 25D1.16 mAb validated the specificity of our labeling conditions, as labeling with 25D1.16 was only detected in MVA-OVA–infected cells (Supplemental Fig. 1B). The K^bOVAp complexes in the infected EL4 cells appeared in a small number of discrete patches (Fig. 2A). In contrast, EL4 cells incubated with soluble synthetic OVAp showed a broader pattern of staining for K^bOVAp, although the distribution of fluorescence was not homogeneous (Fig. 2A). Taking only into account the patches of highest intensity, there were significantly fewer in infected cells than in cells incubated with soluble peptide (Fig. 2B, *upper left panel*). We also made a quantitative comparison between the overall K^bOVAp distribution on the extracellular membrane of MVA-OVA–infected and OVAp-incubated EL4 cells. This quantification is based on the concept of IPR (28), commonly used in quantum material science to ascertain the degree in which a material behaves as a metal or an insulator. Intensity profiles of the 25D1.16 labeling (Fig. 2B, *upper middle panel*) were generated using the Fiji platform (27), and normalized values of these intensities were used as input for NIPR. The value of the NIPR is 1 for a perfectly homogeneous distribution and approaches 0 in a distribution with a single peak (see *Materials and Methods* for a detailed description and justification of the use of this concept). The MVA-OVA–infected cells had a significantly lower NIPR value than did the OVAp-incubated cells (Fig. 2B, *upper right panel*), providing quantitative evidence for the visual observations of the more discrete K^bOVAp distribution in virus-infected cells as compared with peptide-incubated cells (Fig. 2A, *upper row*). The different pattern of K^bOVAp distribution between virus-infected and OVAp-incubated EL4 cells excluded the possibility that the observed patches were an artifact of the staining protocol. The expression level and distribution of the total pool of K^b molecules were indistinguishable between virus-infected, peptide-incubated, and untreated EL4 cells, as shown by flow cytometry, confocal microscopy, and NIPR quantification (Fig. 2A, 2B, *lower panels*). This indicated that the MVA-OVA virus did not cause major perturbations of MHC class I expression at the plasma membrane and therefore did not explain the discrete distribution of K^bOVAp observed upon infection. This was furthermore corroborated by confocal analysis and quantification of the distribution of K^bOVAp complexes on EL4 cells infected with MVA-OVA and EL4 cells infected with the parental MVA (MVA-WT) virus and simulta-

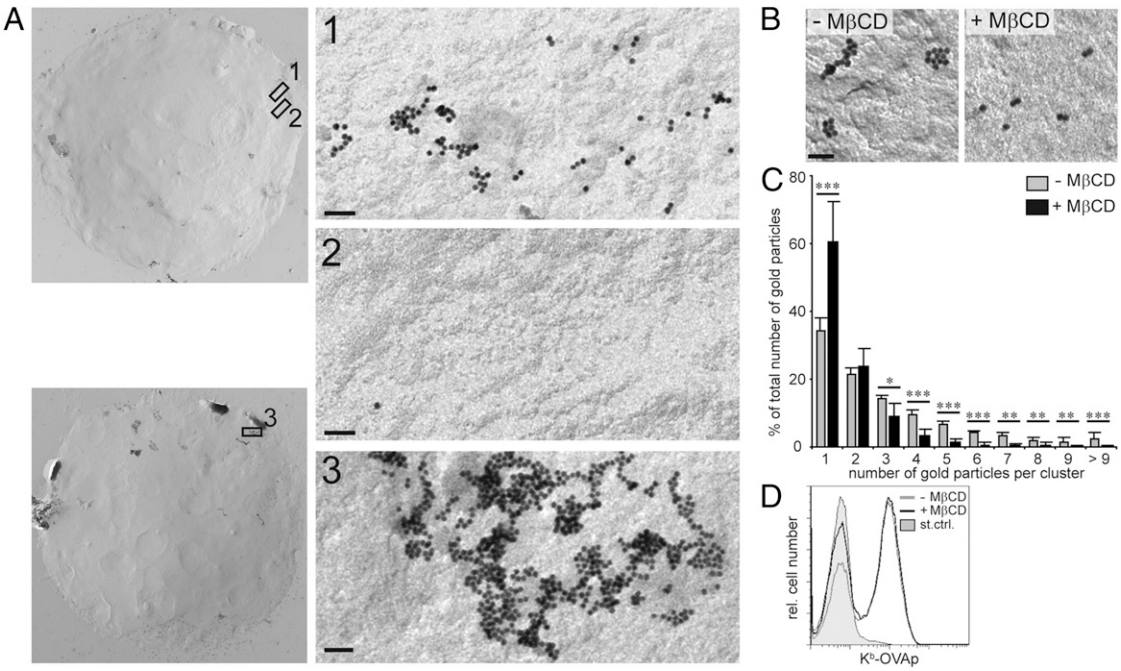

FIGURE 3. Cholesterol-dependent clusters of closely associated K^bOVAp complexes at the cell surface of MVA-OVA–infected EL4 cells. (**A**) Transmission electron microscopy images of replicas of two MVA-OVA–infected EL4 cells (10 PFU/cell) labeled with the 25D1.16 Ab. Amplifications of the numbered regions are shown on the right. Images were taken at magnification of 10,000 (upper cell) and 8,000 (lower cell). Scale bars: cells, 2 μm; details, 50 nm. (**B**) Details of replicas from MVA-OVA–infected EL4 cells treated or mock treated with methyl-β-cyclodextrin and labeled with the 25D1.16 mAb. Scale bars: 50 nm. (**C**) Quantification of gold cluster size on replicas of methyl-β-cyclodextrin–treated and mock-treated EL4 cells labeled with the 25D1.16 mAb. Data, representative of two experiments, show means ± SD of the quantification of 14 treated cells (8,796 gold particles) and five mock-treated cells (14,543 gold particles). Statistical significance of differences was calculated with a two-tailed, unpaired Student *t* test. (**D**) Expression level of K^bOVAp complexes on EL4 cells treated or mock treated with methyl-β-cyclodextrin as measured by 25D1.16 staining and flow cytometry (gated on live cells).

neously incubated with graded amounts of the soluble synthetic OVAp (Supplemental Fig. 2). MVA-WT–infected and OVAp-treated EL4 cells showed a broad distribution of K^bOVAp, indistinguishable from EL4 cells treated with OVAp alone.

Labeling with 25D1.16 of MVA-OVA–infected and soluble OVAp-pulsed primary bone marrow–derived dendritic cells also showed a marked difference in the distribution of K^bOVAp patches (Fig. 2C). This indicated that the formation of cognate pMHC patches also occurred in physiologically relevant APCs and suggested that this was a general phenomenon.

We finally compared the distribution of K^bOVAp complexes at the cell surface of EL4 cells infected with MVA-OVA and E.G7-OVA cells (19), EL4-derived cells that constitutively express full-length OVA. In E.G7-OVA cells the K^bOVAp distribution was quite contiguous (Fig. 2D), very much as observed for the soluble OVAp-incubated EL4 cells (see Fig. 2A and Supplemental Fig. 2B). Therefore, the discrete patches of K^bOVAp observed in MVA-OVA–infected EL4 cells was not merely the result of endogenous expression and antigenic processing of the OVA protein, but was related to the process of viral infection.

Molecular resolution of cognate pMHC clusters

The limited resolution of the confocal microsope did not permit an estimation of the distances between individual K^bOVAp complexes within the discrete patches observed in the MVA-OVA–infected cells. We therefore performed electron microscopy analysis of cell surface replicas prepared from EL4 cells that had been infected with MVA-OVA, fixed with paraformaldehyde, and labeled with the 25D1.16 mAb. Clusters with directly apposed gold particles could readily be detected (Fig. 3A, *inset 1*), indicating that the distance between individual K^bOVAp complexes was $\leq$10 nm. Cluster size generally ranged from 4 to 20 particles. There were membrane areas devoid of K^bOVAp clusters (e.g., Fig. 3A, *inset 2*) whereas in other areas clusters tended to group together (Fig. 3A, *inset 1*). In a few replicas we detected very large clusters of more than a hundred gold particles (Fig. 3A, *inset 3*) that, based on their size, could correspond to the patches observed by confocal microscopy.

We previously showed that TCR nanoclusters are disrupted when cholesterol is extracted from the cell surface membrane with methyl-β-cyclodextrin (8). Treatment of MVA-OVA–infected EL4 cells with 5 mM methyl-β-cyclodextrin for 30 min at 37°C prior to fixation and labeling of the cells resulted likewise in a clear reduction in K^bOVAp cluster size (Fig. 3B, 3C). The reduction was not due to removal of the K^bOVAp complexes from the cell surface membrane, as the intensity of 25D1.16 labeling measured by flow cytometry did not change upon treatment (Fig. 3D). The integrity of the K^bOVAp clusters was therefore dependent on the presence of cholesterol in the plasma membrane. Additionally, even though cells were fixed before labeling with 25D1.16 and all procedures were performed on ice to prevent K^bOVAp clustering being provoked by the labeling procedure, the effect of methyl-β-cyclodextrin treatment totally excluded this possibility.

Enrichment for cognate pMHC clusters correlates with enhanced stimulatory capacity

We compared EL4 cells infected with MVA-OVA and EL4 cells infected with the parental MVA virus and incubated with graded amounts of soluble OVAp for their ability to stimulate K^b-restricted, OVAp-specific OT-1 T cells (23). We measured the level of K^bOVAp expression on a small aliquot of each EL4 population by flow cytometry (Fig. 4A). The remaining cells were cocultured for 2 d with the OT-1 T cells, after which the percentage of IFN-γ–producing OT-1 T cells was quantified by flow cytometry. The level of K^bOVAp expression on each EL4 population was plotted against the percentage of IFN-γ–producing OT-1 T cells induced by that EL4 population (Fig. 4B). At identical densities of K^bOVAp at the cell surface EL4 cells infected with MVA-OVA were much more potent inducers of IFN-γ production by the OT-1 T cells than were MVA-infected EL4 cells loaded with soluble exogenous peptide. Hence, these data show a correlation between the degree of pMHC clustering and increased stimulatory capacity.

Discussion

These findings are relevant for understanding the mechanisms for TCR signaling. The detection of clusters of MHC molecules

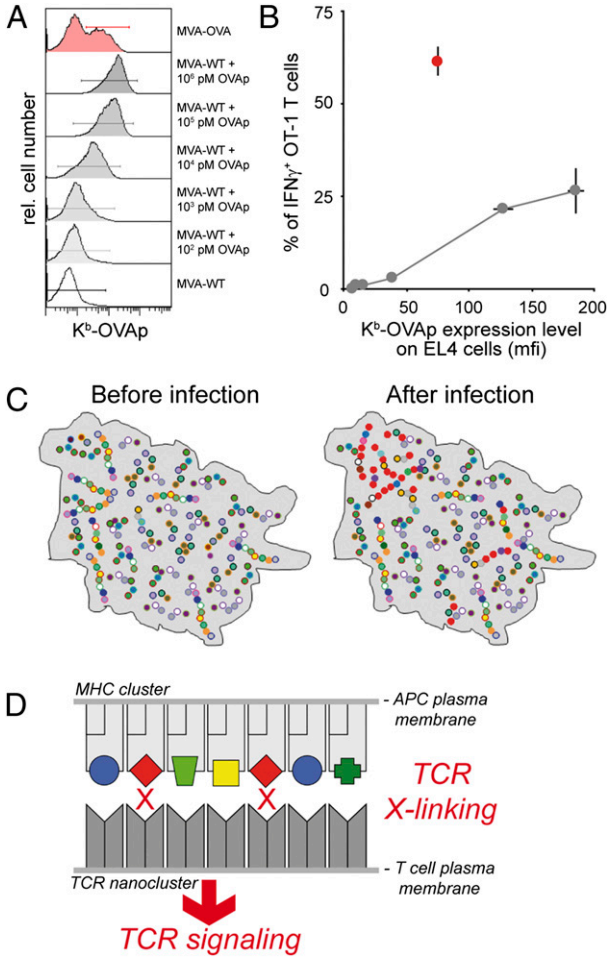

FIGURE 4. Comparison of stimulatory capacity of MVA-OVA–infected and OVAp-incubated EL4 cells. (**A**) K^bOVAp density on the cell surface of EL4 cells infected with MVA-OVA (10 PFU/cell) and EL4 cells infected with MVA-WT (10 PFU/cell) and incubated with graded amounts of soluble OVAp. Cells were stained with the 25D1.16 mAb and analyzed by flow cytometry. (**B**) In vitro activation of OT-1 T cells by MVA-OVA–infected EL4 cells and EL4 cells infected with MVA-WT and incubated with OVAp. The percentage (mean ± SD of triplicate cultures) of OT-1 T cells producing IFN-γ, measured by intracellular staining and flow cytometry, was plotted against the level of K^bOVAp expression (mean ± SD of triplicate samples) by the Ag-presenting EL4 cells (as shown in (**A**)). Data from one of three experiments are shown. (**C**) Model of pMHC distribution before and after virus infection. In noninfected cells MHC molecules (represented by individual dots) within clusters present a large variety of peptides (indicated by different colors of dots). Upon infection, clusters enriched for MHC molecules presenting viral peptides (red dots) can be detected at the cell surface. (**D**) Model of multivalent engagement between MHC nanoclusters and TCR nanoclusters. The MHC nanoclusters need to contain minimally two agonistic Ag peptide molecules (in red) to be able to trigger the TCR.

presenting identical viral peptides upon virus infection provides a solution to the paradox between the long-known need for multivalency of experimental, activating TCR ligands (Abs, pMHC oligomers) and the notion that there is only a very small probability that a few identical pMHC complexes within a sea of irrelevant pMHC complexes will ever get close enough to engage the TCR in a multivalent fashion (Fig. 4C). Second, they support a model where the interaction between the TCR and its pMHC ligands is multivalent, providing a mechanism whereby cooperation between low-affinity interactions leads to an increased apparent affinity and thus high sensitivity (Fig. 4D) (33). Our data are in agreement with a recently published paper (34) in which it was shown by optical microscopy that infection of fibroblasts with vaccinia virus also leads to the accumulation of cognate pMHC complexes in patches at the plasma membrane and that this distribution correlated with increased stimulatory capacity. Our data expand these finding by showing that pMHC patching also occurs in physiologically relevant APCs, that is, primary bone marrow–derived dendritic cells, and, more importantly, by showing that cognate pMHC complexes are indeed contacting each other, forming a supramolecular structure or cluster.

The analysis by electron microscopy of replicas of MVA-OVA–infected cells labeled with the 25D1.16 mAb permits us to get an estimate of the distance between individual K^bOVAp complexes within the clusters. The diameter of the gold conjugate used in this study (10 nm) is approximately twice the lateral dimensions of the $\alpha_1\alpha_2$ peptide–binding domain of the pMHC complex (4×5 nm^2) (30). Because we can resolve directly adjacent gold particles in the clusters, this would mean that the distance between individual K^bOVAp complexes should not be >5 nm. It may even be less, considering on the one hand that each 25D1.16 mAb has two binding sites for the K^bOVAp complex, and on the other hand that steric hindrance between the protein A-gold conjugates and a labeling efficiency of $<100\%$ might not allow detection of all K^bOVAp complexes within a cluster. These distances are in the range of the estimated diameter of the TCR complex (35) and spacing of individual TCR complexes within TCR nanoclusters (7, 8). The cognate pMHC clusters could therefore facilitate multivalent interactions with TCR nanoclusters that in turn could give rise to the enhanced T cell response we observed.

K^bOVAp-positive clusters are dependent on cholesterol for their integrity. Transport of proteins from the *trans*-Golgi network to the cell surface depends on cholesterol-enriched carriers (36), and it would thus be expected that the K^bOVAp complexes that arrived at the cell surface in the first hours after infection would be enriched in these cholesterol-rich cell surface domains. The more important implication is that delivery of this already K^bOVAp-enriched composition at the cell surface is indicative of intracellular enrichment. In agreement with this, Lu et al. (34) could indeed detect cognate pMHC clusters as far down the secretory pathway as the *cis*-Golgi. The exact mechanism causing the cognate pMHC enrichment remains unclear but it may result from the burst of viral protein expression that peaks a few hours postinfection. This burst could lead to a preferential loading of newly synthesized MHC class I complexes with viral peptides. This burst of viral protein expression is general to all viruses. In the case of vaccinia virus and its MVA derivative, a likely additional mechanism is that these viruses, as many others, generate their own replication center in the cytoplasm and recruit endoplasmic reticulum membranes to this structure (37). It is therefore possible that endogenous MHC class I molecules that are inserted upon cotranslational translocation into endoplasmic reticulum membranes surrounding a viral replication center will likely be confronted with virally derived peptides. Such spatiotemporal considerations may also explain the differences in K^bOVAp distribution between MVA-OVA–infected EL4 cells and the E.G7-OVA cells. The OVA protein in E.G7-OVA cells is continuously and, most likely, ubiquitously expressed. Therefore, the K^bOVAp distribution we observe in these cells represents a steady-state situation, with K^bOVAp complexes with a wide range of residence times at the cell surface. Some K^bOVAp complexes should have just reached the cell surface and would be still present in the cholesterol-enriched surface domains. These would be responsible for the more intense patches observed in these cells. Longer residing K^bOVAp complexes may over time have leaked out of these domains, giving rise the "interstitial" labeling between the patches. In contrast, infection of EL4 cells with MVA-OVA leads to a temporally and possibly spatially constrained OVA expression. At the time of analysis the K^bOVAp complexes at the cell surface have reached the cell surface recently and would be expected to be still enriched in the cholesterol-enriched cell surface domains. The spatial constraint of OVA expression would reduce the number of K^bOVAp patches at the cell surface.

Our results do not resolve whether the cognate pMHC clusters exclusively contain cognate pMHC complexes. If this were the case, it would be interesting from a cell biological point of view, as it might shed light on potential mechanisms responsible for sorting individual MHC class I molecules based on their peptide cargo. However, it might be less relevant with regard to T cells, as long as the spacing of individual cognate pMHC molecules does not exceed a critical distance. In vitro studies with artificial TCR ligands are compatible with the existence of such spacing constraints on T cell activation (38).

In summary, our data show that clusters of cognate class I pMHC can form under immunologically relevant conditions in primary cells and cell lines. Such clusters may explain why T cells can respond with high sensitivity to Ag even though the receptor–ligand interactions that induce this response are of low affinity.

Note added in proof. After submission of this manuscript, P. Roche et al. published a paper in which it was shown that clusters of cognate-peptide MHC class II molecules can be detected at the cell surface of dendritic cells upon uptake of Ag (39).

Acknowledgments

We thank the personnel of the Optical and Confocal Microscopy, Electron Microscopy, and Flow Cytometry facilities of the Centro Biología Molecular Severo Ochoa for expert help.

Disclosures

The authors have no financial conflicts of interest.

References

1. Demotz, S., H. M. Grey, and A. Sette. 1990. The minimal number of class II MHC-antigen complexes needed for T cell activation. *Science* 249: 1028–1030.
2. Harding, C. V., and E. R. Unanue. 1990. Quantitation of antigen-presenting cell MHC class II/peptide complexes necessary for T-cell stimulation. *Nature* 346: 574–576.
3. Irvine, D. J., M. A. Purbhoo, M. Krogsgaard, and M. M. Davis. 2002. Direct observation of ligand recognition by T cells. *Nature* 419: 845–849.
4. Corr, M., A. E. Slanetz, L. F. Boyd, M. T. Jelonek, S. Khilko, B. K. al-Ramadi, Y. S. Kim, S. E. Maher, A. L. Bothwell, and D. H. Margulies. 1994. T cell receptor-MHC class I peptide interactions: affinity, kinetics, and specificity. *Science* 265: 946–949.
5. Matsui, K., J. J. Boniface, P. A. Reay, H. Schild, B. Fazekas de St Groth, and M. M. Davis. 1991. Low affinity interaction of peptide-MHC complexes with T cell receptors. *Science* 254: 1788–1791.
6. Weber, S., A. Traunecker, F. Oliveri, W. Gerhard, and K. Karjalainen. 1992. Specific low-affinity recognition of major histocompatibility complex plus peptide by soluble T-cell receptor. *Nature* 356: 793–796.
7. Kumar, R., M. Ferez, M. Swamy, I. Arechaga, M. T. Rejas, J. M. Valpuesta, W. W. Schamel, B. Alarcon, and H. M. van Santen. 2011. Increased sensitivity of antigen-experienced T cells through the enrichment of oligomeric T cell receptor complexes. *Immunity* 35: 375–387.
8. Schamel, W. W., I. Arechaga, R. M. Risueño, H. M. van Santen, P. Cabezas, C. Risco, J. M. Valpuesta, and B. Alarcón. 2005. Coexistence of multivalent and

monovalent TCRs explains high sensitivity and wide range of response. *J. Exp. Med.* 202: 493–503.
9. Boniface, J. J., J. D. Rabinowitz, C. Wülfing, J. Hampl, Z. Reich, J. D. Altman, R. M. Kantor, C. Beeson, H. M. McConnell, and M. M. Davis. 1998. Initiation of signal transduction through the T cell receptor requires the multivalent engagement of peptide/MHC ligands. *Immunity* 9: 459–466.
10. Kaye, J., and C. A. Janeway, Jr. 1984. The Fab fragment of a directly activating monoclonal antibody that precipitates a disulfide-linked heterodimer from a helper T cell clone blocks activation by either allogeneic Ia or antigen and self-Ia. *J. Exp. Med.* 159: 1397–1412.
11. Anderson, H. A., E. M. Hiltbold, and P. A. Roche. 2000. Concentration of MHC class II molecules in lipid rafts facilitates antigen presentation. *Nat. Immunol.* 1: 156–162.
12. Hiltbold, E. M., N. J. Poloso, and P. A. Roche. 2003. MHC class II-peptide complexes and APC lipid rafts accumulate at the immunological synapse. *J. Immunol.* 170: 1329–1338.
13. Jenei, A., S. Varga, L. Bene, L. Mátyus, A. Bodnár, Z. Bacsó, C. Pieri, R. Gáspár, Jr., T. Farkas, and S. Damjanovich. 1997. HLA class I and II antigens are partially co-clustered in the plasma membrane of human lymphoblastoid cells. *Proc. Natl. Acad. Sci. USA* 94: 7269–7274.
14. Kropshofer, H., S. Spindeldreher, T. A. Röhn, N. Platania, C. Grygar, N. Daniel, A. Wölpl, H. Langen, V. Horejsi, and A. B. Vogt. 2002. Tetraspan microdomains distinct from lipid rafts enrich select peptide-MHC class II complexes. *Nat. Immunol.* 3: 61–68.
15. Matko, J., Y. Bushkin, T. Wei, and M. Edidin. 1994. Clustering of class I HLA molecules on the surfaces of activated and transformed human cells. *J. Immunol.* 152: 3353–3360.
16. Fooksman, D. R., G. K. Grönvall, Q. Tang, and M. Edidin. 2006. Clustering class I MHC modulates sensitivity of T cell recognition. *J. Immunol.* 176: 6673–6680.
17. Gorer, P. A. 1950. Studies in antibody response of mice to tumour inoculation. *Br. J. Cancer* 4: 372–379.
18. Schneider, U., H. U. Schwenk, and G. Bornkamm. 1977. Characterization of EBV-genome negative "null" and "T" cell lines derived from children with acute lymphoblastic leukemia and leukemic transformed non-Hodgkin lymphoma. *Int. J. Cancer* 19: 621–626.
19. Moore, M. W., F. R. Carbone, and M. J. Bevan. 1988. Introduction of soluble protein into the class I pathway of antigen processing and presentation. *Cell* 54: 777–785.
20. Lutz, M. B., N. Kukutsch, A. L. Ogilvie, S. Rössner, F. Koch, N. Romani, and G. Schuler. 1999. An advanced culture method for generating large quantities of highly pure dendritic cells from mouse bone marrow. *J. Immunol. Methods* 223: 77–92.
21. El-Gogo, S., C. Staib, M. Meyr, V. Erfle, G. Sutter, and H. Adler. 2007. Recombinant murine gammaherpesvirus 68 (MHV-68) as challenge virus to test efficacy of vaccination against chronic virus infections in the mouse model. *Vaccine* 25: 3934–3945.
22. Drexler, I., K. Heller, B. Wahren, V. Erfle, and G. Sutter. 1998. Highly attenuated modified vaccinia virus Ankara replicates in baby hamster kidney cells, a potential host for virus propagation, but not in various human transformed and primary cells. *J. Gen. Virol.* 79: 347–352.
23. Hogquist, K. A., S. C. Jameson, W. R. Heath, J. L. Howard, M. J. Bevan, and F. R. Carbone. 1994. T cell receptor antagonist peptides induce positive selection. *Cell* 76: 17–27.
24. Parham, P., C. J. Barnstable, and W. F. Bodmer. 1979. Use of a monoclonal antibody (W6/32) in structural studies of HLA-A,B,C, antigens. *J. Immunol.* 123: 342–349.
25. Lopez Guerrero, J. A., J. M. Redondo, B. Alarcón, F. Sánchez-Madrid, M. Rodríguez Moya, M. Ortíz de Landazuri, C. Bernabeu, and M. Fresno. 1989. Different functional domains on the transferrin receptor molecule defined by monoclonal antibodies. *Immunology* 66: 252–257.
26. Porgador, A., J. W. Yewdell, Y. Deng, J. R. Bennink, and R. N. Germain. 1997. Localization, quantitation, and in situ detection of specific peptide-MHC class I complexes using a monoclonal antibody. *Immunity* 6: 715–726.
27. Schindelin, J., I. Arganda-Carreras, E. Frise, V. Kaynig, M. Longair, T. Pietzsch, S. Preibisch, C. Rueden, S. Saalfeld, B. Schmid, et al. 2012. Fiji: an open-source platform for biological-image analysis. *Nat. Methods* 9: 676–682.
28. Castro, M., and F. Domínguez-Adame. 1997. Electric field effects in Fibonacci superlattices. *Phys. Lett. A* 225: 321–325.
29. van der Merwe, P. A., and O. Dushek. 2011. Mechanisms for T cell receptor triggering. *Nat. Rev. Immunol.* 11: 47–55.
30. Bjorkman, P. J., M. A. Saper, B. Samraoui, W. S. Bennett, J. L. Strominger, and D. C. Wiley. 1987. Structure of the human class I histocompatibility antigen, HLA-A2. *Nature* 329: 506–512.
31. Lillemeier, B. F., J. R. Pfeiffer, Z. Surviladze, B. S. Wilson, and M. M. Davis. 2006. Plasma membrane-associated proteins are clustered into islands attached to the cytoskeleton. *Proc. Natl. Acad. Sci. USA* 103: 18992–18997.
32. Sherman, E., V. Barr, S. Manley, G. Patterson, L. Balagopalan, I. Akpan, C. K. Regan, R. K. Merrill, C. L. Sommers, J. Lippincott-Schwartz, and L. E. Samelson. 2011. Functional nanoscale organization of signaling molecules downstream of the T cell antigen receptor. *Immunity* 35: 705–720.
33. Alarcón, B., M. Swamy, H. M. van Santen, and W. W. Schamel. 2006. T-cell antigen-receptor stoichiometry: pre-clustering for sensitivity. *EMBO Rep.* 7: 490–495.
34. Lu, X., J. S. Gibbs, H. D. Hickman, A. David, B. P. Dolan, Y. Jin, D. M. Kranz, J. R. Bennink, J. W. Yewdell, and R. Varma. 2012. Endogenous viral antigen processing generates peptide-specific MHC class I cell-surface clusters. *Proc. Natl. Acad. Sci. USA* 109: 15407–15412.
35. Sun, Z. Y., S. T. Kim, I. C. Kim, A. Fahmy, E. L. Reinherz, and G. Wagner. 2004. Solution structure of the CD3εδ ectodomain and comparison with CD3εγ as a basis for modeling T cell receptor topology and signaling. *Proc. Natl. Acad. Sci. USA* 101: 16867–16872.
36. Ikonen, E., and K. Simons. 1998. Protein and lipid sorting from the *trans*-Golgi network to the plasma membrane in polarized cells. *Semin. Cell Dev. Biol.* 9: 503–509.
37. Miller, S., and J. Krijnse-Locker. 2008. Modification of intracellular membrane structures for virus replication. *Nat. Rev. Microbiol.* 6: 363–374.
38. Minguet, S., M. Swamy, B. Alarcon, I. F. Luescher, and W. W. Schamel. 2007. Full activation of the T cell receptor requires both clustering and conformational changes at CD3. *Immunity* 26: 43–54.
39. Bosch, B., E. L. Heipertz, J. R. Drake, and P. A. Roche. 2013. Major histocompatibility complex (MHC) class II-peptide complexes arrive at the plasma membrane in cholesterol-rich microclusters. *J. Biol. Chem.* 288: 13,236–13,242.

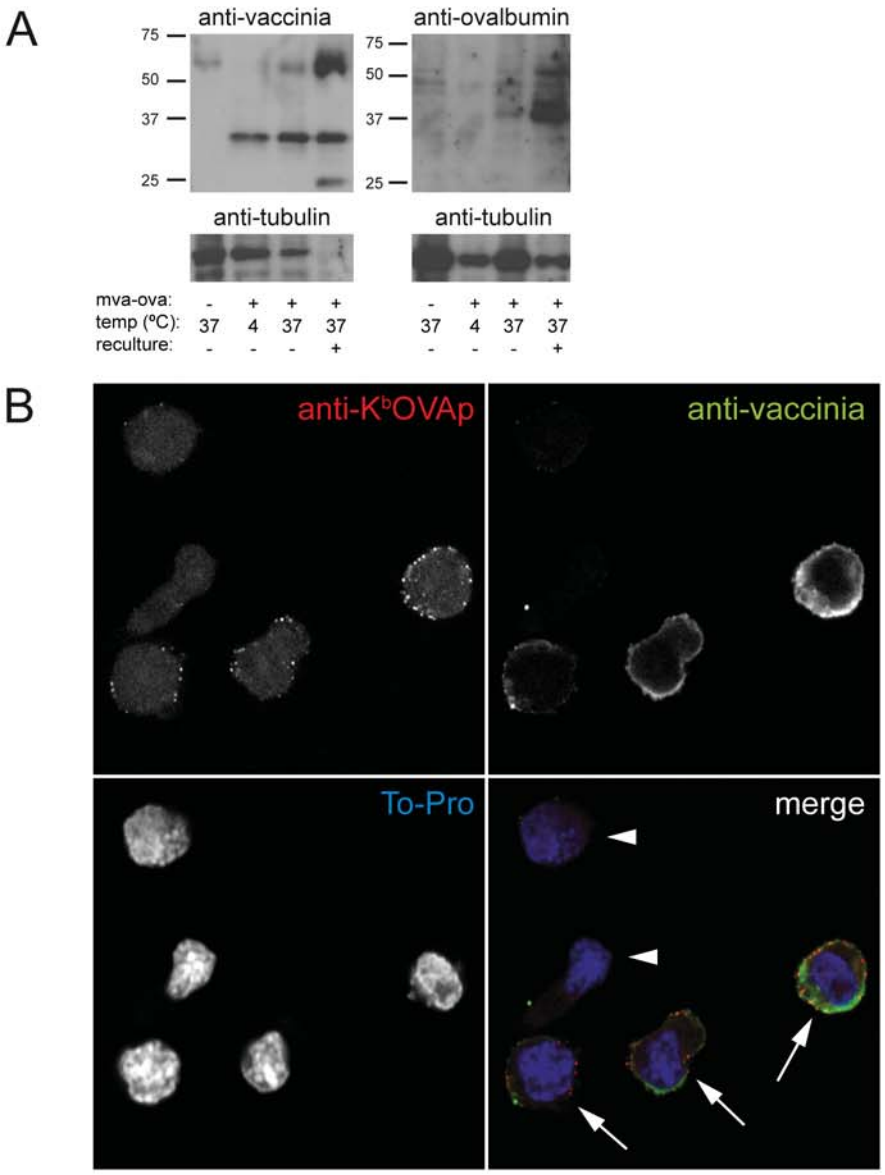

Supplemental figure 1

Infection of EL4 cells by MVA-OVA and specific detection of K^bOVAp complexes in infected cells. A. EL4 cells were incubated with MVA-OVA virus at 10 moi for 1 hour at 4 ºC or 37 ºC. All samples were washed to remove free virus and part of the sample incubated at 37 ºC was recultured for 5 hours at 37 ºC. Cell lysates were prepared and analyzed by SDS-PAGE and immuno-blotting using antisera specific for vaccinia (left panel) or ovalbumin protein (Abcam, Cambridge, UK)(right panel). EL4 cells grown for 1 hour at 37ºC without virus were included as specificity control. A number of virally encoded proteins could be detected whose expression depended on or increased strongly upon reculture, indicating active translation of viral RNAs and thus effective viral infection. B. EL4 cells infected for 6 hours with MVA-OVA at 10 moi and then labeled with the 25D1.16 mAb, followed by permeabilization and staining with a vaccinia antiserum and To-Pro. A representative mid-plane optical section obtained via confocal microscopy is shown. Infected cells are identified by white arrows and non-infected cells by white arrow heads.

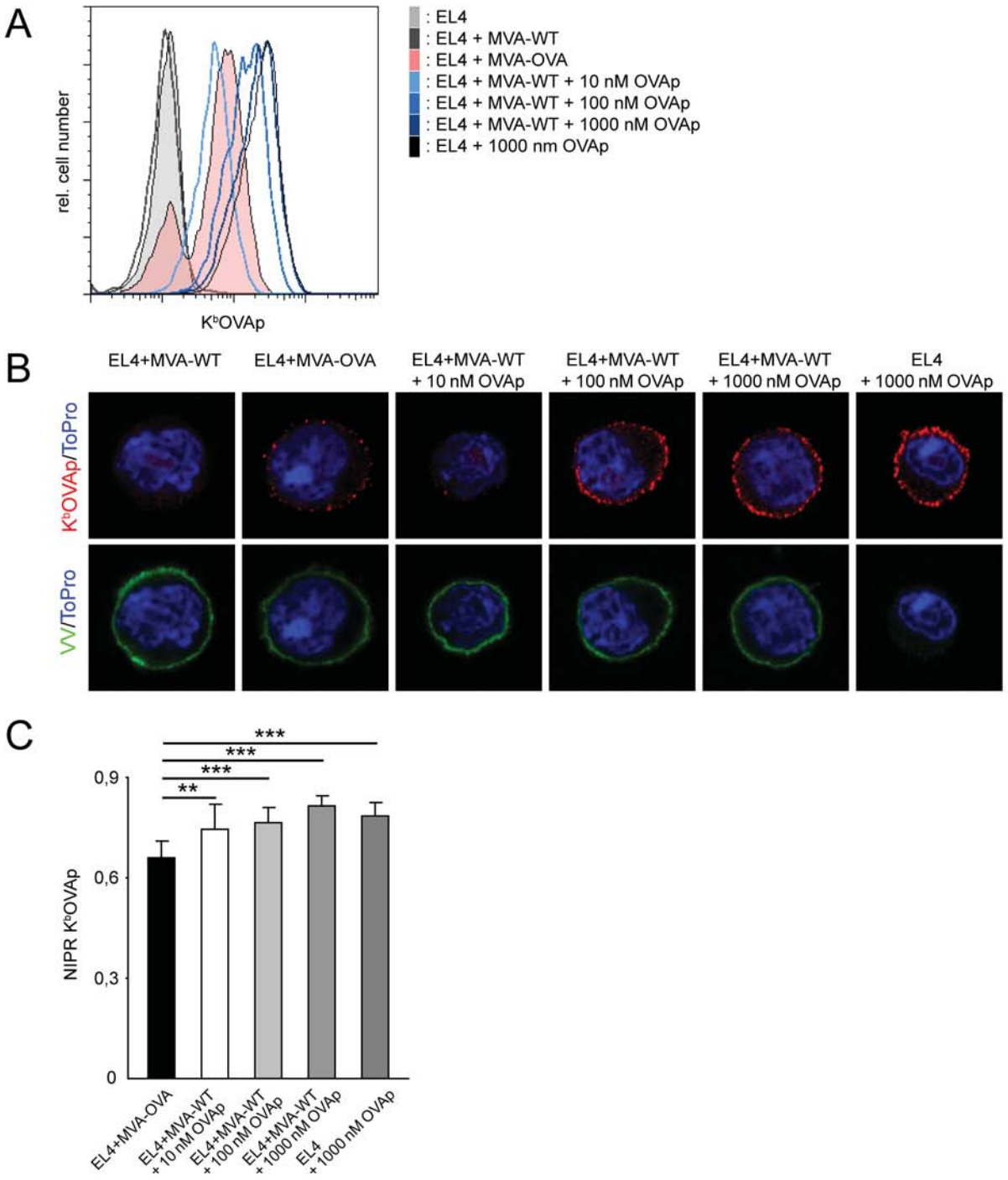

Supplemental figure 2

K^bOVAp distribution at the cell surface of EL4 cells after viral infection and incubation with soluble OVAp. A. Level of K^bOVAp expression at the cell surface of EL4 cells infected with the indicated viruses with or without co-incubation with graded amounts of OVAp, measured by staining with the 25D1.16 mAb and flow cytometry analysis. B. Distribution of K^bOVAp complexes on the same panel of cells, detected by double-staining with the 25D1.16 mAb (red) and vaccinia antiserum (green) under non-permeabilizing conditions and analysis by confocal microscopy. Representative mid-plane sections are shown. Note that, even though EL4 cells infected with MVA-WT and co-incubated with 10 nM OVAp have almost similar levels of expression as the MVA-OVA infected cells (panel A), immunofluorescence staining is barely detected, in agreement with the notion that the distribution of K^bOVAp is more homogeneous on these cells as compared to the MVA-OVA infected cells. C. Quantification of the distribution of K^bOVAp complexes via the NIPR for 12 cells of each of the indicated groups. Statistical differences were calculated with a 2-tailed Student T test (** $p<0.01$; *** $p<0.001$).